ATLAS NOTE

ATL-PHYS-PUB-2015-051

2nd December 2015

Early Inner Detector Tracking Performance in the 2015 Data at $\sqrt{s} = 13$ TeV

The ATLAS Collaboration

Abstract

This note summarises the studies undertaken to recommend benchmark values and systematic uncertainties for various aspects of the ATLAS Inner Detector tracking based on $\sqrt{s} = 13$ TeV proton-proton collisions from the Large Hadron Collider Run 2 data. The track reconstruction efficiency, fake rate, and related systematic uncertainties are presented for two different track quality selections, along with the impact parameter resolution and the alignment weak mode systematic uncertainities. These recommendations apply to physics analyses using Inner Detector tracks in Run 2 data and are important inputs for other objects based on tracks.

ATL-PHYS-PUB-2015-051
02 December 2015

1 Introduction

The ATLAS detector [1] is a multi-purpose detector at the Large Hadron Collider (LHC). The Inner Detector (ID) [2] of the ATLAS experiment is responsible for efficiently and accurately measuring charged particle trajectories (tracks) in the region of ATLAS closest to the interaction point. This allows precise detemination of the momentum and impact parameters (transverse and longitudinal distances of closest approach to a reference point) of charged particles, as well as the positions of primary and secondary vertices. It comprises three subsystems based on different detector technologies: the Pixel detector (Pixel), Semiconductor Tracker (SCT) and Transition Radiation Tracker (TRT).

During the first LHC Long Shutdown, the Pixel system underwent significant updates; a new smaller beam pipe was installed together with a new innermost Pixel layer, called the Insertable B-Layer (IBL) [3] which allows measurements closer to the interaction point. In addition, new Pixel Service Quarter Panels [4], providing more robust service connections and allowing the recovery of a number of inactive pixel modules, were installed.

In this note, the studies undertaken to provide a recommended set of Inner Detector tracking performance benchmarks are summarised. These recommendations provide information on appropriate working points (track selection criteria with well-understood performance) to be used in Run 2 physics analyses using ID tracks, along with the estimated systematic uncertainties from a variety of sources which should be applied. The data set and simulation samples used for these studies and the selections applied to the reconstructed tracks are discussed in Sections 2 and 3, respectively. In Section 4 the track reconstruction efficiencies are presented for two different track quality selections. In Section 5 the fake rate evaluation is shown. In Sections 6 and 7 the alignment weak modes and impact parameter resolution analyses are discussed, respectively.

2 Data Set and Simulation Samples

The results presented in this note were obtained by using data collected at the LHC in proton-proton collisions at $\sqrt{s}$ = 13 TeV.

- For the fake rate study in Section 5 data taken between September and November 2015 are used, corresponding to an integrated luminosity of around 1.74 fb^{-1}. In this period, the bunch spacing was 25 ns and the average number of interactions per bunch crossing, μ, reached approximately 23. A zero-bias trigger[1] was used to select the data events for study.
- The alignment weak mode measurements in Section 6 use data from the same period as above, selected using a logical OR of all physics triggers.
- The analysis of the impact parameter resolutions presented in Section 7 uses data taken in June 2015, corresponding to an integrated luminosity of around 0.37 nb^{-1}. In this period, the bunch spacing was 50 ns, and μ was approximately 0.005. The events used were selected by the minimum bias trigger, which requires hits in the Minimum Bias Trigger Scintillators [5].

[1] This trigger selects events one LHC orbit after a reference trigger, to give a completeley unbiased sample of collision events.

Appropriate data quality requirements are applied to all data sets such that only events from periods with good detector performance are included.

Monte Carlo (MC) models are used to evaluate the track reconstruction efficiency and to compare data to simulation. The PYTHIA 8 [6] generator was used to produce samples for these studies. This generator uses a model that splits the total inelastic cross section for inclusive hadron-hadron collisions into three components: non-diffractive, single diffractive and double diffractive. The ATLAS minimum-bias tune A2, based on MSTW2008LO PDF is used [7]. For studying the fake rate, a varying number of such events were overlaid on top of an 'empty' event, produced by simulating events containing single neutrinos, in order to provide simulated 'pile-up' events (events containing multiple proton-proton interactions) with a range of values of μ. In addition, for impact parameter resolution and weak mode studies a sample of Z bosons decaying into muon pairs was used. This sample was generated with POWHEG [8–10] with dedicated modeling of single boson production [11], interfaced to PYTHIA 8 for showering. The detector response is simulated in a detailed model implemented in GEANT4 [12].

The detector geometries used for the simulated samples are the standard geometry used as baseline for the production of MC simulation in 2015 (referred to as *default*) and an updated geometry which adds some additional material to better model the physical IBL staves (referred to as *updated*). The difference in the tracking efficiency due to the changes between the two geometries has been evaluated to be negligible. The *default* geometry was used for the production of Monte Carlo samples unless otherwise specified. The uncertainty on the tracking efficiency is dominated by the knowledge of the ID material distribution, therefore, based on the ID material studies described in [13], a number of distorted geometries were produced and used in order to study this source of uncertainty:

- +5%*Extra* = same as *default*, but with 5% extra material uniformily distributed in the ID.
- +25%*PixServExtra* = same as *default*, but with 25% extra material uniformily distributed in the Pixel services regions.
- +50%*PixServExtra* = same as *default*, but with 50% extra material uniformily distributed in the Pixel services regions.
- +10%*IBLExtra* = same as *updated*, but with 10% extra material uniformily distributed in the IBL region.

3 Selection

Reconstructed tracks are selected by applying track quality criteria. Two sets of quality criteria are studied in this note, based on transverse momentum (p_{T}), pseudorapidity[2] (η) and the number of hits in the subsystems.

Loose

- $p_{\mathrm{T}} > 400$ MeV
- $|\eta| < 2.5$

[2] ATLAS uses a right-handed coordinate system with its origin at the nominal interaction point (IP) in the centre of the detector and the z-axis along the beam pipe. The x-axis points from the IP to the centre of the LHC ring, and the y-axis points upward. Cylindrical coordinates (r, ϕ) are used in the transverse plane, ϕ being the azimuthal angle around the beam pipe. The pseudorapidity is defined in terms of the polar angle θ as $\eta = -\ln\tan(\theta/2)$.

- Number of Pixel and SCT clusters on track ('silicon hits') ≥ 7
- Number of shared modules ≤ 1
- Number of silicon holes ≤ 2
- Number of pixel holes ≤ 1

Tight Primary (in addition to the Loose selection requirements)

- Number of silicon hits ≥ 9 (if $|\eta| \leq 1.65$)
- Number of silicon hits ≥ 11 (if $|\eta| \geq 1.65$)
- At least one hit on one of the two innermost pixel layers
- No pixel holes

A shared hit is a hit used by more than one track. A Pixel module is considered to be shared if it has one or more shared hits. In the case of the SCT, a shared module has at least two shared hits[3]. Holes are defined as intersections of the reconstructed track trajectory with a sensitive detector element that do not result in a hit - essentially a 'missing hit' on a track. They are estimated by following closely the track trajectory and comparing the hits-on-track with the intersected modules. Inactive modules or regions such as edge areas on the silicon sensors are excluded from the hole definition. The tracks selected by the above working points can have extensions into the TRT, but no explicit criteria are applied on the number of TRT hits.

The Loose track selection corresponds to the default track requirements applied during 'inside-out' track reconstruction [14] and aims to obtain highly efficient charged particle reconstruction at the cost of a non-negligible fraction of fake tracks. The name Tight Primary reflects the fact that this set of criteria is designed and optimized for selecting primary tracks, which are defined in Section 4, and rejecting fake tracks at the cost of a reduced track reconstruction efficiency. Further details are discussed in Sections 4 and 5.

4 Tracking Efficiency

The track reconstruction efficiency is evaluated from simulation using a hit-based track-to-truth particle association to associate reconstructed tracks to primary particles [15]. Each of the clusters is associated to the truth particle which has the largest energy deposition in the MC simulation. The clusters are then weighted according to their importance in the track reconstruction: if the clusters are from the pixel detector including IBL, the weight is set to 10 for each cluster. If they are from the SCT, the weight is set to 5 and if they are from the TRT, the weight is set to 1. A weighted matching probability P_{match} can be defined using the ratio of the number of hits which are common to a given track and the corresponding truth particle ($N^{\text{common}}_{\text{Pixel, SCT, TRT}}$) and the number of hits which form the track ($N^{\text{track}}_{\text{Pixel, SCT, TRT}}$):

$$P_{\text{match}} = \frac{10 \cdot N^{\text{common}}_{\text{Pixel}} + 5 \cdot N^{\text{common}}_{\text{SCT}} + 1 \cdot N^{\text{common}}_{\text{TRT}}}{10 \cdot N^{\text{track}}_{\text{Pixel}} + 5 \cdot N^{\text{track}}_{\text{SCT}} + 1 \cdot N^{\text{track}}_{\text{TRT}}}. \quad (1)$$

[3] No requirement is made that the two hits should be on opposite sides of the double-sided modules.

The hit-matching technique is very robust since it exploits the relation between tracks and truth particles at the GEANT4 energy deposition level and is mostly independent of the detector resolutions. A $P_{\text{match}} > 0.5$ is required for a primary track.

Primary charged particles are defined as charged particles with a mean lifetime $\tau > 300$ ps, either directly produced in proton-proton interactions or from decays of directly produced particles with mean lifetime $\tau < 30$ ps. Particles produced from decays of particles with $\tau > 30$ ps are denoted secondary particles and are excluded [15].

The tracking efficiency $\epsilon_{\text{trk}}(p_{\text{T}}, \eta)$ is then measured as a function of p_{T} and η with the following definition:

$$\epsilon_{\text{trk}}(p_{\text{T}}, \eta) = \frac{N_{\text{rec}}^{\text{matched}}(p_{\text{T}}, \eta)}{N_{\text{gen}}(p_{\text{T}}, \eta)} \tag{2}$$

where p_{T} and η are truth particle properties, $N_{\text{rec}}^{\text{matched}}(p_{\text{T}}, \eta)$ is the number of reconstructed tracks matched to truth charged particles and $N_{\text{gen}}(p_{\text{T}}, \eta)$ is the number of truth charged particles in that (p_{T}, η) range.

The tracking efficiency for primary tracks is shown in Figure 1 as a function of p_{T} and η for both Loose and Tight Primary selections, as defined in Section 3.

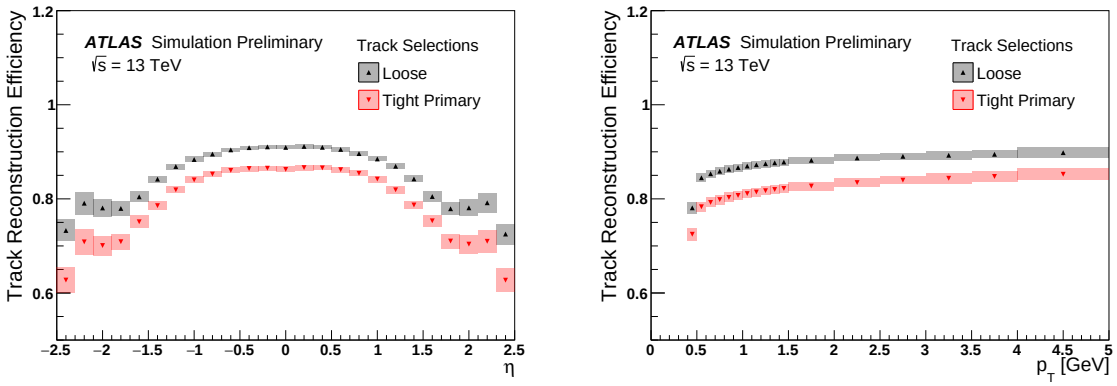

(a) (b)

Figure 1: Track reconstruction efficiency, evaluated by using minimum bias simulated events, as a function of truth η (a) and p_{T} (b) for Loose and Tight Primary track selections.The bands indicate the total systematic uncertainty.

The evaluated Tight Primary track reconstruction efficiency is overall lower (up to ~ 10% for $1.5 \leq |\eta| \leq 2.5$, ~ 5% for $|\eta| < 1.5$ and ~ 5% in the full p_{T} range) than the Loose track reconstruction efficiency because of the more stringent requirements, but the Tight Primary selection improves fake rejection, as detailed in Section 5. In general, the lower track reconstruction efficiency in the region $|\eta| > 1$ is due to the increasing amounts of material that the particles must traverse. The slight increase in efficiency for $|\eta| > 2$ is due to the particles passing through a larger number of sensitive layers. Above $p_{\text{T}} \geq 5$ GeV, the track reconstruction efficiency reaches a plateau equal to ~90% and ~85% respectively for the Loose and Tight Primary selections.

Track Reconstruction Efficiencies and Systematic Uncertainties				
Track Quality Selection	Loose		Tight Primary	
η Range	$\lvert\eta\rvert \leq 0.1$	$2.3 \leq \lvert\eta\rvert \leq 2.5$	$\lvert\eta\rvert \leq 0.1$	$2.3 \leq \lvert\eta\rvert \leq 2.5$
Track Reconstruction Efficiency	91%	73%	86%	63%
$\mathrm{Sys}_{+5\%Extra}$	0.4%	0.9%	0.5%	1.1%
$\mathrm{Sys}_{PixServExtra}$	—	2.0%	—	2.3%
$\mathrm{Sys}_{+30\%IBLExtra}$	0.2%	0.5%	0.2%	0.5%
Total Systematic Uncertainty	0.4%	2.2%	0.5%	2.6%

Table 1: Track reconstruction efficiencies and absolute systematic uncertainties for both Loose and Tight Primary track quality selections. Two η intervals were selected to demonstrate the range of the systematic uncertainties: $|\eta| \leq 0.1$ (which is characterised by the lowest systematic uncertainty values) and $2.3 \leq |\eta| \leq 2.5$ (which is characterised by the largest systematic uncertainty values). The total systematic uncertainty is estimated by quadratically combining the three different contrbutions: $\mathrm{Sys}_{+5\%Extra}(\mathrm{p_T}, \eta)$, $\mathrm{Sys}_{PixServExtra}(\mathrm{p_T}, \eta)$ and $\mathrm{Sys}_{+30\%IBLExtra}(\mathrm{p_T}, \eta)$. The results shown are obtained by integrating over p_{T} in the range [0.4,20] GeV.

The accuracy with which the amount of material in the ID is known is the largest source of uncertainty on the simulation-based estimate of the track reconstruction efficiency. There are currently three main components to the systematic uncertainty (referred to as $\mathrm{Sys}_{+5\%Extra}(\mathrm{p_T}, \eta)$, $\mathrm{Sys}_{PixServExtra}(\mathrm{p_T}, \eta)$ and $\mathrm{Sys}_{+30\%IBLExtra}(\mathrm{p_T}, \eta)$ in the following) designed to cover disagreements between data and MC simulation in the context of the ID material studies described in [13]. These components have been evaluated for both Loose and Tight Primary selections as a function of p_{T} and η by subtracting unity from the ratio of the track reconstruction efficiencies measured in the default and distorted geometry samples listed in Section 2:

$$\mathrm{Sys}_{ExtraMaterial}(\mathrm{p_T}, \eta) = \frac{\epsilon_{\mathrm{trk}}^{default}(\mathrm{p_T}, \eta)}{\epsilon_{\mathrm{trk}}^{ExtraMaterial}(\mathrm{p_T}, \eta)} - 1 \tag{3}$$

where *ExtraMaterial* means +5%*Extra*, +25%*PixServExtra*, +50%*PixServExtra* or +10%*IBLExtra*.

The contribution $\mathrm{Sys}_{+5\%Extra}(\mathrm{p_T}, \eta)$ is directly measured from the +5%*Extra* sample, to cover the systematic uncertainty due to an overall 5% material mis-modeling which is the assumed upper limit on the precision with which the Run 1 material budget is known. Based on the hadronic interactions and photon conversions studies [13], the contribution $\mathrm{Sys}_{+10\%IBLExtra}(\mathrm{p_T}, \eta)$ corresponding to the results from the +10%*IBLExtra* sample, was increased by a factor of 3 to fully cover the disagreement between data and simulation, and so becomes $\mathrm{Sys}_{+30\%IBLExtra}(\mathrm{p_T}, \eta)$. An uncertainty denoted $\mathrm{Sys}_{PixServExtra}(\mathrm{p_T}, \eta)$ is applied in the region with $|\eta| > 1.5$ to cover the data/simulation discrepancy in the forward region of the detector. For $1.5 < |\eta| < 2.3$, the full difference between the default and +50%*PixServExtra* samples is conservatively used to evaluate this contribution to the systematic uncertainty, while, in the region $|\eta| > 2.3$, since the missing pixel services material is estimated to be in the order of 30% [13], it is necessary to carry out a linear interpolation between the +25%*PixServExtra* and +50%*PixServExtra* samples to evaluate the uncertainty.

The errors bars shown in Figure 1 represent the total systematic uncertainty obtained by combining in quadrature the three contributions discussed above. An overview of the track reconstruction efficiency and the absolute values of the systematic uncertainties is shown in Table 1.

With a fraction higher than 98%, pions represent the dominant particle type in the simulation samples used to evaluate the track reconstrunction efficiency. Therefore, since the track reconstruction efficiency is sensitive to particle type, the above-described track systematic uncertainties are intended to be applied to charged pions.

5 Fake Rate

Not all tracks reconstructed in the ID will correspond closely to a charged particle traversing the detector; in particular, combinatorial effects which increase with pile-up can give rise to so-called 'fake' tracks. To provide a cross-check on the modelling of the tracking fake rate, an estimate of this quantity is made by assuming that the number of 'genuine' (i.e. non-fake) tracks is to first order proportional to the number of pile-up interactions. Any deviation from linearity is therefore assumed to be due to fakes. Figure 2(a) shows the average number of tracks passing the Loose and Tight Primary selections, as a function of μ.

The data in Figure 2(a) are fit with a linear function $f(\mu) = m\mu$ in the region $10 \leq \mu \leq 15$ in which both data and Monte Carlo demonstrate approximately linear behaviour. The relative deviation from the linear fit:

$$\frac{\langle N_{\text{tracks}} \rangle(\mu) - f(\mu)}{\langle N_{\text{tracks}} \rangle(\mu)}$$

provides an estimate of the fake rate, which is shown in Figure 2(b). It is a relative measure, and by construction close to zero in the region of the fit, $10 \leq \mu \leq 15$. In approximating the fake rate in this manner, we assume that the contribution from fake tracks is negligible in the fit region; this is a more reliable assuption for the Tight Primary track selection than the Loose. This method also assumes that the tracking efficiency is independent of μ, and that the fake contribution from sources other than pile-up combinatorics are negligible; these latter two assumptions have been verified to hold in Monte Carlo. The Tight Primary track selection is estimated to have a smaller fake rate, which is also more stable versus μ, than the Loose selection. The recommended systematic uncertainty to be applied on the fake rate is 50%, which is typical of the size of the differences between Data and MC seen in these studies.

6 Weak Modes

The alignment of the Inner Detector is based on tracking information and minimizes hit-to-track residuals with respect to alignment parameters using a least squares principle [16]. The procedure inherently suffers from so-called *weak modes* of the solution which are detector deformations under which the χ^2 of the track fit remains invariant. The weak mode deformations may, in general, affect reconstructed parameters of the tracks [17].

So far, only three types of biases on reconstructed track parameters have been considered to be relevant for physics results:

1. Charge-antisymmetric momentum bias, i.e. bias on the reconstructed Q/p due to sagitta distortion: $Q/p \longrightarrow Q/p + \delta_{\text{sagitta}}$ (see [18] for details).
2. Bias on the reconstructed transverse impact parameter: $d_0 \longrightarrow d_0 + \delta_{d_0}$.
3. Bias on the reconstructed longitudinal impact parameter: $z_0 \longrightarrow z_0 + \delta_{z_0}$.

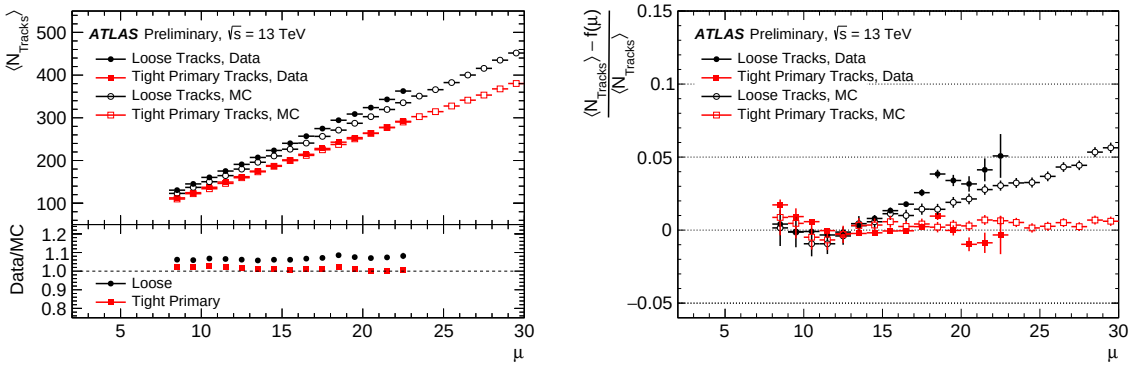

(a) (b)

Figure 2: Average number of reconstructed tracks as a function of μ for data and minimum bias simulation, applying the Loose and Tight Primary selections (a), and an estimation of the tracking fake rate, derived from the deviation from linearity of a fit to N_{tracks} as a function of μ (b). In (a), the statistical uncertainty on the mean number of tracks is considered, but are too small to be seen. The displayed μ range for data, in contrast to simulation, is limited by the available μ values in the data sample.

The biases listed above were assessed using an iterative method described in [17, 18]. A data set of around 130,000 $Z \to \mu\mu$ event candidates were selected as described in [19], taken from a data period with stable Inner Detector conditions. However, with run-dependent alignment corrections in place, the results extracted from this selected period are representative of the entire 25 ns data set.

Figure 3 shows the $\eta - \phi$ map of the sagitta distortion. The η projection of the map and the Root Mean

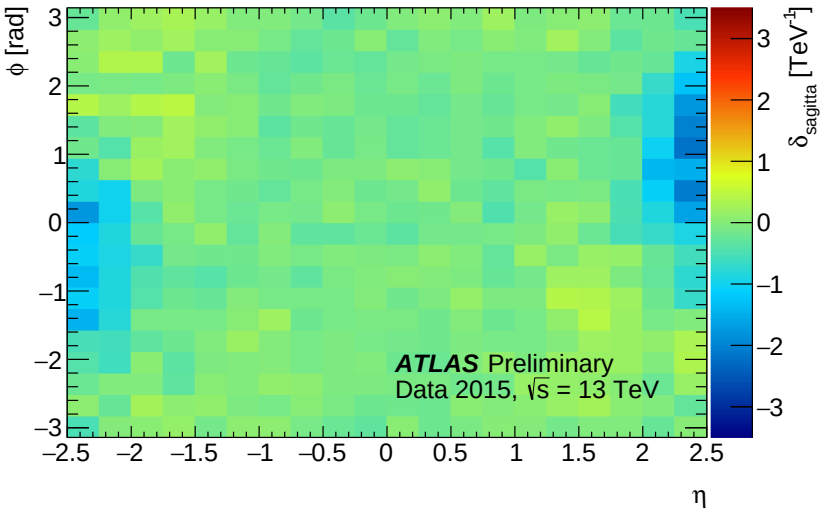

Figure 3: $\eta - \phi$ map of the sagitta distortion (δ_{sagitta}) as reconstructed from $Z \to \mu\mu$ events.

Squared (RMS) spread in each η bin are shown in Figures 4(a) and 4(b), respectively. It is worth noting that the ϕ variation of the bias (represented by the RMS) is usually of similar order as the mean value

from the projection on η. When integrated over the entire ID acceptance, the mean sagitta distortion is -0.17 TeV^{-1}, but the absolute value does not exceed 0.1 TeV^{-1} over a large part of the acceptance ($|\eta| < 2$).

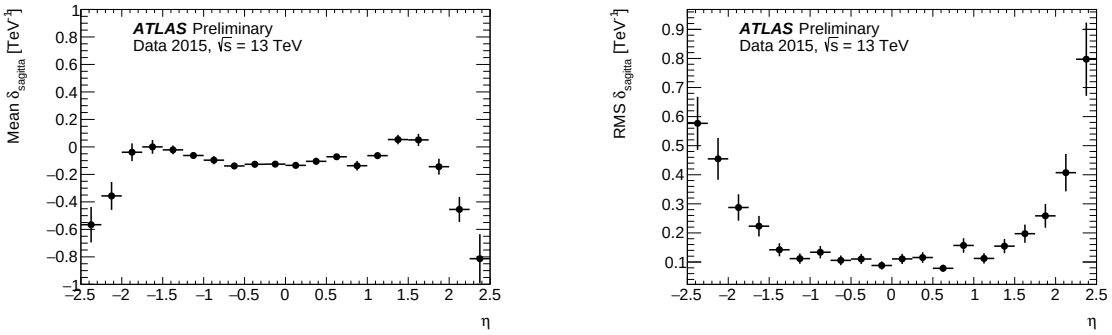

(a) (b)

Figure 4: Projection on η of the mean (a) and RMS spread (b) of the $\eta - \phi$ δ_{sagitta} distortion map (Figure 3).

Figures 5 and 7 show the analogous 2D maps for the δ_{d_0} and δ_{z_0} biases, respectively. Similarly, Figures 6 and 8 show the mean value and RMS projections on η of the δ_{d_0} and δ_{z_0} biases, respectively.

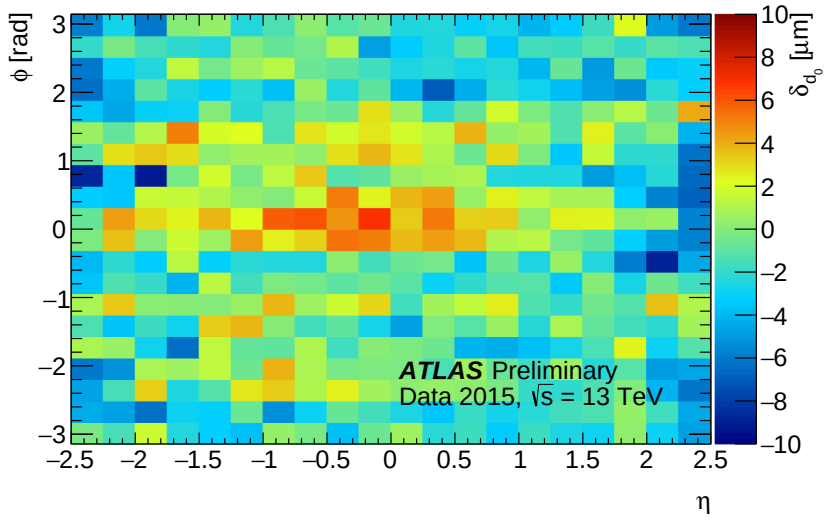

Figure 5: $\eta - \phi$ map of the δ_{d_0} distortion as reconstructed from $Z \to \mu\mu$ events.

The systematic effect due to the alignment-induced bias is assessed by altering the reconstructed tracks parameters using the above $\eta - \phi$ distortion maps.

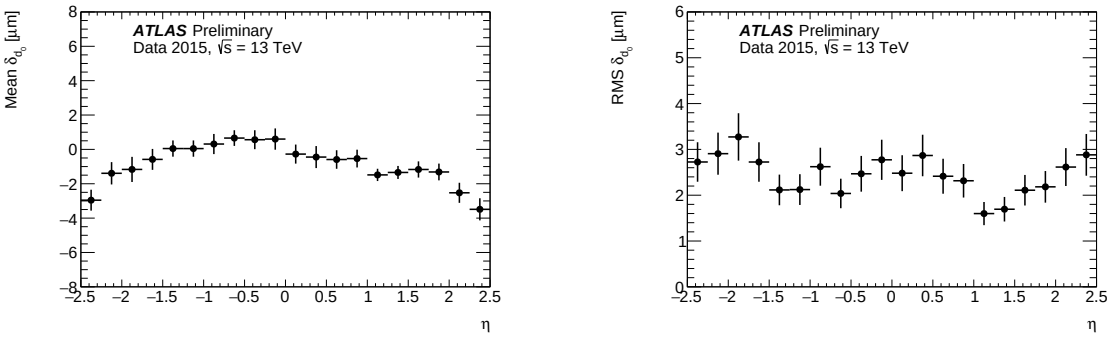

(a) (b)

Figure 6: Projection on η of the mean (a) and RMS spread (b) of the $\eta - \phi$ δ_{d_0} distortion map (Figure 5).

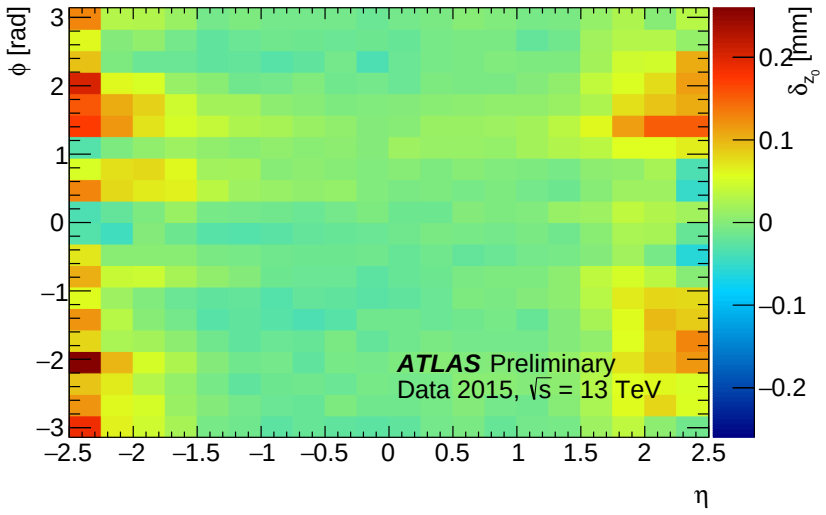

Figure 7: $\eta - \phi$ map of the δ_{z_0} distortion as reconstructed from $Z \to \mu\mu$ events.

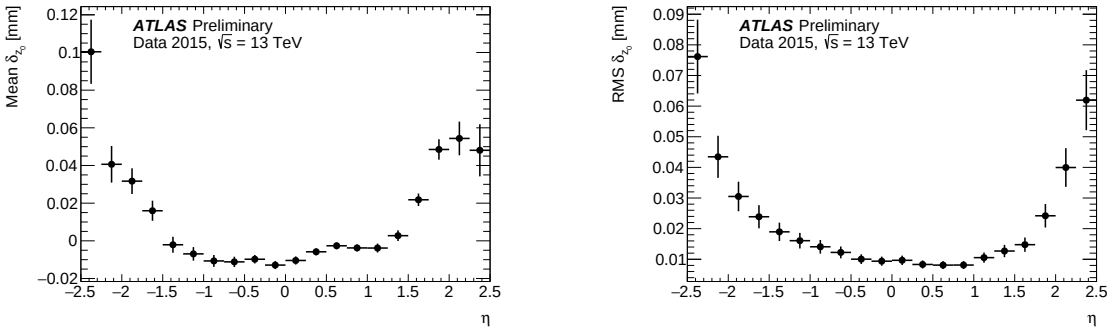

(a) (b)

Figure 8: Projection on η of the mean(a) and RMS spread (b) of the $\eta - \phi$ δ_{z_0} distortion map (Figure 7).

7 Impact Parameter Resolution

The transverse and longitudinal impact parameters, d_0 and z_0 respectively, are important to discriminate tracks originating from primary vertices from tracks originating from secondary vertices. The primary vertices are used as the reference point for the distance of closest approach. The intrinsic resolutions of the track impact parameters with respect to the primary vertex are measured from data and simulation. To extrapolate the systematic uncertainty on the impact parameters to higher track p_{T}, the results from minimum bias simulation are compared with those using muon tracks from Z boson decays.

For minimum bias data and simulation, events are required to have a reconstructed primary vertex with at least 10 tracks, while events with one or more additional reconstructed primary vertices with more than 4 tracks are removed to reduce the influence of pile-up. For $Z \to \mu\mu$ simulation, the event selection is described in [19]. To extract the resolutions, the distribution of impact parameters is fitted within 2σ of its mean with a Gaussian function for each bin in η and p_{T} of tracks. In data, the width of the Gaussian function includes the contribution from the uncertainty on the position of the reconstructed primary vertices. The intrinsic resolutions of tracks are obtained by deconvolving the primary vertex uncertainty using the iterative deconvolution procedure [20]. In simulation, the values of the resolutions are calculated from the difference between the reconstructed impact parameters and those of the Monte Carlo truth particles. The values of σ representing the intrinsic resolution are shown in Figure 9. The resolutions from simulation with the nominal and June-2015 alignment [21] in $Z \to \mu\mu$ configurations are also shown. The nominal alignment configuration represents a perfectly aligned detector, while the June-2015 alignment configuration reproduces the uncertainties on this alignment by applying error scalings (random, Gaussian-distributed misalignments with their σ corresponding to the relevant alignment uncertainties) to the various detector components.

The d_0 and z_0 resolutions in both simulations agree with each other to within 20%. The difference of the resolutions between minimum bias data and simulation is taken to be the systematic uncertainty on the impact parameter resolutions. The systematic uncertainties are obtained by taking the square root of the quadrature difference between data and simulation in regions where there are sufficient statistics. A parameterization of the resolutions as a function of η and p_T is used to extrapolate up to higher p_{T} regions which are statistically limited. $Z \to \mu\mu$ offers a cross-check of the validity of the extrapolations into these regions.

8 Conclusions

The behaviour of several important aspects of Inner Detector tracking performance, specifically tracking efficiency, fake rate, alignment weak modes and impact parameter resolution, have been studied in 13 TeV LHC Run 2 data and Monte Carlo simulations. For the tracking efficiencies and fake rates, two working points were considered: the Loose and Tight Primary track quality selections. Based on these studies a series of benchmarks, including paramterizations of the metrics investigated and associated systematic uncertainties, have been derived.

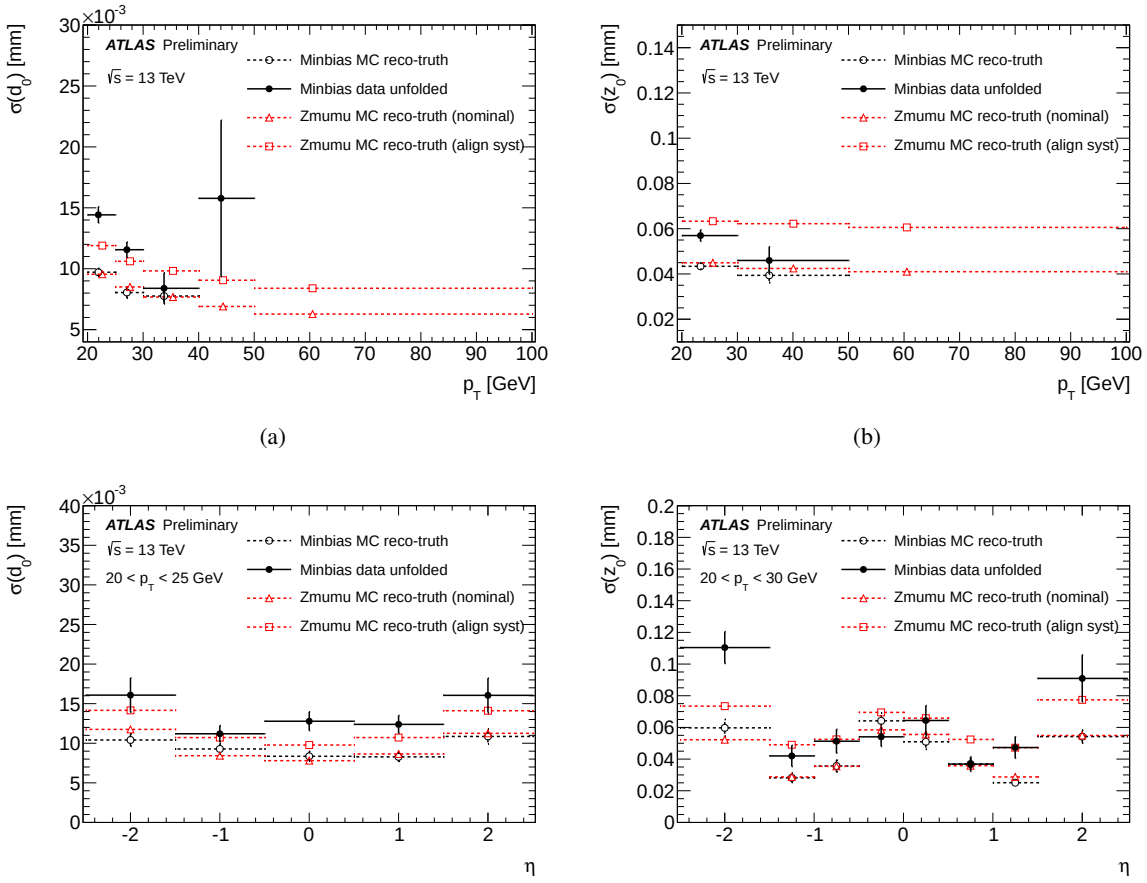

Figure 9: Unfolded transverse (a)(c) and longitudinal (b)(d) impact parameter resolution measured in data as a function of p_{T} and η, compared to the expectation from minimum bias and $Z \to \mu\mu$ simulation. For simulation, the resolution is taken from the differences between the reconstructed and truth quantities (reco-truth) while for data the resolution is derived by using the iterative deconvolution procedure. In the $Z \to \mu^+\mu^-$ simulation, the *nominal* shows the resolutions with perfect alignment configuration, while the *align syst* shows those with the June-2015 alignment configuration, which reproduces the uncertainties on this alignment by applying Gaussian-distributed misalignments to the various detector components. The d_0 and z_0 resolutions in both simulations agree with each other to within 20%.

References

[1] ATLAS Collaboration, *The ATLAS Experiment at the CERN Large Hadron Collider*, JINST **3** (2008) S08003.

[2] ATLAS Collaboration, *ATLAS inner detector: Technical Design Report, 1*, Technical Design Report ATLAS, Geneva: CERN, 1997, URL: https://cds.cern.ch/record/331063.

[3] ATLAS Collaboration, *ATLAS Insertable B-Layer Technical Design Report*, CERN-LHCC-2010-013. ATLAS-TDR-19, Geneva, 2010, URL: https://cds.cern.ch/record/1291633.

[4] Y. Takubo, *The Pixel Detector of the ATLAS experiment for the Run2 at the Large Hadron Collider*, JINST **10**.02 (2015) C02001, arXiv: 1411.5338 [physics.ins-det].

[5] A. Sidoti, *Minimum Bias Trigger Scintillators in ATLAS Run II*, Journal of Instrumentation **9**.10 (2014) C10020, URL: http://stacks.iop.org/1748-0221/9/i=10/a=C10020.

[6] T. Sjostrand, S. Mrenna and P. Z. Skands, *A Brief Introduction to PYTHIA 8.1*, Comput. Phys. Commun. **178** (2008) 852, arXiv: 0710.3820 [hep-ph], URL: https://inspirehep.net/record/764903.

[7] ATLAS Collaboration, *Summary of ATLAS Pythia 8 tunes*, ATL-PHYS-PUB-2012-003, 2012, URL: https://cds.cern.ch/record/1474107.

[8] P. Nason, *A New method for combining NLO QCD with shower Monte Carlo algorithms*, JHEP **11** (2004) 040, arXiv: hep-ph/0409146 [hep-ph], URL: http://stacks.iop.org/1126-6708/2004/i=11/a=040.

[9] S. Frixione, P. Nason and C. Oleari, *Matching NLO QCD computations with Parton Shower simulations: the POWHEG method*, JHEP **11** (2007) 070, arXiv: 0709.2092 [hep-ph], URL: http://inspirehep.net/record/760769.

[10] S. Alioli et al., *A general framework for implementing NLO calculations in shower Monte Carlo programs: the POWHEG BOX*, JHEP **06** (2010) 043, arXiv: 1002.2581 [hep-ph], URL: http://inspirehep.net/record/845712.

[11] S. Alioli et al., *NLO vector-boson production matched with shower in POWHEG*, JHEP **0807** (2008) 060, arXiv: 0805.4802 [hep-ph], URL: http://inspirehep.net/record/787440.

[12] Agostinelli, S, et al., *Geant4 - a simulation toolkit*, Nuclear Instruments and Methods **A 506** (2003) 250, URL: http://inspirehep.net/record/593382.

[13] ATLAS Collaboration, *Studies of the ATLAS Inner Detector material using $\sqrt{s}$ =13 TeV pp collision data*, ATL-PHYS-PUB-2015-050, 2015, URL: https://cds.cern.ch/record/2109010.

[14] T. Cornelissen et al., *The new ATLAS track reconstruction (NEWT)*, J. Phys. Conf. Ser. **119** (2008) 032014, URL: http://stacks.iop.org/1742-6596/119/i=3/a=032014.

[15] ATLAS Collaboration, *Charged-particle distributions in $\sqrt{s}$ = 13 TeV pp interactions measured with the ATLAS detector at the LHC*, ATLAS-CONF-2015-028, 2015, URL: https://cds.cern.ch/record/2037701.

[16] ATLAS Collaboration, *Common Framework Implementation for the Track-Based Alignment of the ATLAS Detector*, ATL-SOFT-PUB-2014-003, 2014, URL: https://cds.cern.ch/record/1670354.

[17] ATLAS Collaboration, *Study of alignment-related systematic effects on the ATLAS Inner Detector tracking*, ATLAS-CONF-2012-141, 2012, URL: https://cds.cern.ch/record/1483518.

[18] ATLAS Collaboration, *Alignment of the ATLAS Inner Detector and its Performance in 2012*, ATLAS-CONF-2014-047, 2014, URL: https://cds.cern.ch/record/1483518.

[19] ATLAS Collaboration, *Study of the mechanical stability of the ATLAS Insertable B-Layer*, ATL-INDET-PUB-2015-001, 2015, URL: https://cds.cern.ch/record/2022587.

[20] ATLAS Collaboration, *Tracking Studies for b-tagging with 7 TeV Collision Data with the ATLAS Detector*, ATLAS-CONF-2010-070, 2010, URL: http://cdsweb.cern.ch/record/1281352.

[21] ATLAS Collaboration, *Alignment of the ATLAS Inner Detector with the initial LHC data at $\sqrt{s}$ = 13 TeV*, ATL-PHYS-PUB-2015-031, 2015, URL: http://cds.cern.ch/record/2038139.